Journal of Materials Science: Materials in Electronics (2019) 30:8502–8507
https://doi.org/10.1007/s10854-019-01170-x

Substantial enhancement of mechanical properties for SnSe based composites with potassium titanate whiskers

Junchao Li[1] · Bo Duan[1] · Jialiang Li[1] · Zheng Ruan[1] · Tao Gao[1] · Zhou Fang[1] · Guodong Li[1,2] · Pengcheng Zhai[1,2] · Gang Chen[1]

Received: 6 January 2019 / Accepted: 18 March 2019 / Published online: 26 March 2019

Abstract
Highly dense p-type polycrystalline SnSe dispersed with x vol% $K_2Ti_6O_{13}$ whiskers ($x = 0$, 1, 3, 5) were fabricated by a high-pressure sintering (HPS) method. The effects of the $K_2Ti_6O_{13}$ whiskers additives on the thermoelectric as well as mechanical properties of the composites were characterized in detail. The electrical conductivity, Seebeck coefficient, and thermal conductivity were measured within the temperature range of 300–830 K. It was found that the $K_2Ti_6O_{13}$ whiskers were distributed homogeneously throughout the matrix and contacted with the SnSe grains intimately. Mechanical properties, such as Vickers hardness, flexural strength, compressive strength and fracture toughness of the composites were improved significantly. Especially, upon the addition of 5 vol% $K_2Ti_6O_{13}$ whiskers, the flexural strength and compressive strength were almost doubled as compared to $K_2Ti_6O_{13}$-free samples. Such substantial enhancement of mechanical properties is an important benefit for the commercial application of thermoelectric devices.

1 Introduction

Many IV–VI compounds have good thermoelectric (TE) performances, such as PbTe [1], PbSe [2], and SnTe [3]. However, the expensiveness of Te and the toxicity of Pb restrict their scale-up commercial applications. SnSe with earth-abundant and environmentally friendly elements has attracted wide attention. As the most potential candidate for next generation TE, p-type single crystal SnSe has a world-record peak *ZT* of about 2.6 at 923 K along the b-axis [4]. Unlike its analogs with a NaCl structure, SnSe crystallizes in a layered structure in the orthorhombic *Pnma* space group below 810 K [5, 6]. The different Se–Sn layered substructures are linked with weaker Sn–Se bonding, which creates a path that slip easily between Se–Sn layered substructures and results in poor mechanical properties [4, 7]. The ideal strength (0.59 GPa) [7] of SnSe is much lower than that of other high-performance thermoelectric materials such as Mg_2Si (4.54 GPa) [8], $CoSb_3$ (7.17 GPa) [9], and TiNiSn (10.52 GPa) [10].

Mechanical properties are vital for the commercial use of the thermoelectric materials since the TE modules are subjected to various mechanical and thermal stresses during the operation. So far, there are few experimental reports on the mechanical properties of polycrystalline SnSe [11–13]. Previous research has shown that incorporating additives with high strength and high elastic modulus, such as nano-particles or nano-wires, is a good method to improve the mechanical properties and is widely used in TE [14, 15], ceramics [16, 17], and alloys [18, 19]. These significant enhancements can be attributed to the pinning effect, fiber bridging and fiber pull-out mechanisms in the matrix particles, which creates mechanically interlocked interfaces between the additives and the matrix. The crack may deflect where the crack tip meets the additives, thus increasing the ability to resist crack growth [16, 17, 20]. Potassium titanate whiskers ($K_2Ti_6O_{13}$) are promising reinforcement materials due to their excellent mechanical properties (Mohs hardness: 4; strength: 7 GPa; modulus: 280 GPa) and other properties (ultralow thermal conductivity: 0.054 W/mK at room temperature; thermal stability: melting point 1643 K; lower

✉ Bo Duan
duanboabc@126.com

✉ Gang Chen
cg_chen@whut.edu.cn

[1] Hubei Key Laboratory of Theory and Application of Advanced Materials Mechanics, Wuhan University of Technology, Wuhan 430070, China

[2] State Key Laboratory of Advanced Technology for Materials Synthesis and Processing, Wuhan University of Technology, Wuhan 430070, China

coefficient of thermal expansion: 6.8×10^{-6} K^{-1}; smaller mass density: 3.3 g/cm^3; lower cost and good dispersibility). $K_2Ti_6O_{13}$ has been widely used as a reinforcement material in polymers [21], metals [18], insulation materials [22], and friction materials [23].

In this work, $K_2Ti_6O_{13}$ whiskers were selected as the reinforcement phase. Different fractions of $K_2Ti_6O_{13}$ whiskers were introduced into the polycrystalline SnSe. High energy ball milling and ultrasonic dispersion were used to disperse the whiskers uniformly in the matrix. The influences of $K_2Ti_6O_{13}$ whiskers on microstructure, and TE and mechanical properties of the composites were investigated systematically.

2 Experimental section

2.1 Sample preparation

Polycrystalline SnSe were synthesized by conventional melting of stoichiometric amounts of tin (Sn, 99.9%) and selenium (Se, 99.999%). The raw materials were sealed into evacuated quartz tubes and kept at 1223 K for 10 h. The obtained ingots were ground into powders with an agate mortar. Commercially available $K_2Ti_6O_{13}$ whiskers (diameter: ~50 nm; length: 0.5–3 μm) were selected as the additives. After ultrasound dispersed in alcohol, the x vol% $K_2Ti_6O_{13}$ whiskers ($x=0$, 1, 3, 5) were mixed with the SnSe powders using a vario-planetary ball mill at 200 rpm for 2 h. The obtained mixtures were consolidated by HPS at 623 K for 7 min under 2.5 GPa. Subsequently, samples were cut into appropriate sizes for measurements of thermoelectric and mechanical properties.

2.2 Characterization

The densities (d) of the samples were measured by the Archimedes method. The phases were checked by X-ray diffractometry (XRD, Bruker D8 Advance). The microstructures of the fresh fractured surface were characterized by field-emission scanning electron microscopy (FE-SEM, Hitachi SU8020). The electrical conductivities (σ) and Seebeck coefficients (S) were measured by the standard four-probe method (CTA instrument; CRY-ALL) under a He atmosphere from 300 to 830 K. The thermal diffusivity (λ) was measured by the laser flash method (Netzsch, LFA457). The total thermal conductivity κ_{tol} of the composites was calculated by the formula $\kappa_{tol}=C_p\lambda d$, where $C_p=0.25$ is specific heat [4]. Due to the anisotropic characteristic of SnSe alloys, the thermal and electrical properties are measured in the same direction. The Vickers hardness test was conducted with an indentation force of 2.94 N maintained for 5 s on a hardness tester (HV-1000A). Three-point flexural tests were carried out at room temperature on samples for measurement of the flexural strength using a Z-wick testing system (the bending span was fixed at 8 mm, the strain rate was 2 × 10E-4/s), with size 1.5 × 3 × 12 mm. Compression tests were also carried out using the Z-wick testing system with size 3 × 3 × 6 mm. The fracture toughness of the specimen was measured using the three-points flexural specimen by the single-edge notch beam test. The starting notch with a length of half the width was created at the midspan of the specimen using a diamond-wire saw instrument, and the width of the notch was less than 0.3 mm. The fracture toughness can be calculated with the following equation [24]:

$$K_{IC}=\frac{3PL\sqrt{a\times10^{-3}}}{2bw^2}\left[1.93-3.07\left(\frac{a}{w}\right)+14.53\left(\frac{a}{w}\right)^2-25.07\left(\frac{a}{w}\right)^3+25.08\left(\frac{a}{w}\right)^4\right]$$

where K_{IC} is fracture toughness, P is critical applied load, L is the bending span, b is the thickness, w is the height, and a is the depth of starting notch. At least 12 valid samples were used for each set of tests.

3 Results and discussion

3.1 Phase and microstructure

Powder X-ray diffraction patterns of the SnSe + x vol% $K_2Ti_6O_{13}$ whiskers ($x=0$, 1, 3, 5) samples are shown in

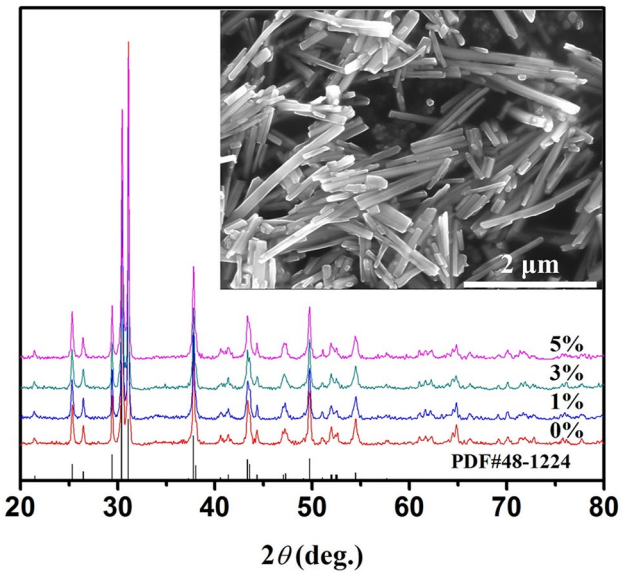

Fig. 1 XRD patterns of SnSe with different amounts of $K_2Ti_6O_{13}$ whiskers. The inset shows the microstructure of $K_2Ti_6O_{13}$ whiskers

Fig. 1. All diffraction peaks can be well indexed to the orthorhombic SnSe phase with a *Pnma* symmetry (PDF #48-1224). Since the $K_2Ti_6O_{13}$ content is very low, the peaks of $K_2Ti_6O_{13}$ were not found in the XRD patterns even for the sample dispersed with 5 vol% $K_2Ti_6O_{13}$. In order to obtain the arbitrary section and reflect the state of $K_2Ti_6O_{13}$ in the matrix more intuitively, the samples used for fracture scanning electron microscopy testing were soaked in liquid nitrogen for 30 min before breaking them. It can be seen from Fig. 2a that there are no cracks or voids in the bulk $K_2Ti_6O_{13}$-free sample. The relative densities of the samples are 97.2%, 96.7%, 96.5% and 96.2%, for $x=0$, 1, 3 and 5, respectively, which decrease slightly with increasing $K_2Ti_6O_{13}$ fraction. The theoretical densities, d_{th} of the composites are calculated using $d_{th}=(1\text{-}x)d_{SnSe}+xd_{K2Ti6O13}$ in which x, d_{SnSe} and $d_{K2Ti6O13}$, are the volume fraction, theoretical density of SnSe (6.18 g/cm^3) and theoretical density of $K_2Ti_6O_{13}$ whiskers (3.3 g/cm^3), respectively. Combined with ball milling and sintered by cubic high pressure apparatus with lower temperature and shorter time, no obvious orientation preference were obtained as shown in Fig. 2a, compared with spark plasma sintering and hot pressure methods [25, 26]. As shown in Fig. 2b–f, it was found that the $K_2Ti_6O_{13}$ whiskers are uniformly dispersed and tightly

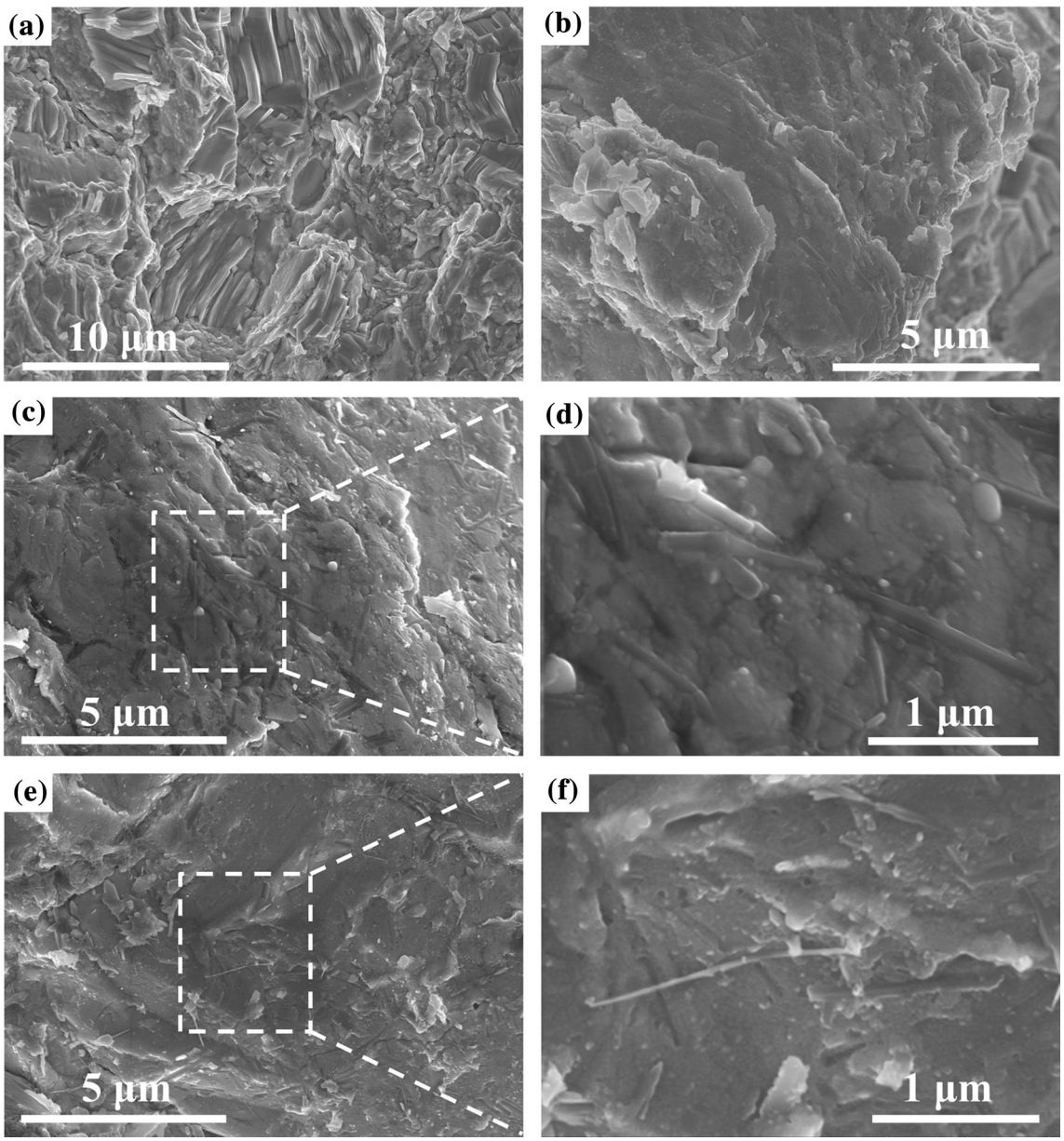

Fig. 2 FE-SEM images of freshly fracture surfaces of SnSe + $K_2Ti_6O_{13}$ whiskers composites: **a** $x=0$ vol%, **b** $x=1$ vol%, **c, d** $x=3$ vol%, and **e, f** $x=5$ vol%

incorporated throughout the matrix, significantly improving the mechanical properties [27–29].

3.2 Thermoelectric properties

Figure 3 shows the temperature dependences of TE properties for the samples. As shown in Fig. 3a, the σ of all samples increase monotonically with increasing temperature, indicative of intrinsic semiconductor transport behavior. As the temperature increases from 300 to 700 K, the σ is very low due to the intrinsically low carrier concentration [4], then increases rapidly to the maximum at a certain temperature. The upturn of the σ should result from the thermal excitation of carriers [4, 30]. The σ of SnSe sintered by HPS is higher than those by other processed routes in literatures [31, 32], which may be attributed to the decreased band gap under high pressure [33, 34], or difference in composition due to the loss and oxidation under different technological conditions. In addition, the σ of the composites is slightly reduced by the addition of $K_2Ti_6O_{13}$, due to the higher electrical resistivity of $K_2Ti_6O_{13}$ (3.3×10^{13} Ω m). The S values for all the samples are positive, as shown in Fig. 3b, indicating that they belong to typical p-type semiconductor. With increasing temperature S decreases in the temperature range of 400–573 K and 673–810 K and increases from 573 to 673 K. A similar temperature dependence trend was observed for the reports [35], but the values were higher. This may be attributed to the increased carrier effective mass induced by high pressure in this work [36].

The lattice thermal conductivity κ_L ($\kappa_L=\kappa_{tol}-\kappa_e$, κ_e is electrical thermal conductivity $\kappa_e=L\sigma T$, $L=1.5\times10^{-8}$ V^2/K^2 is Lorentz number [4]) is shown in Fig. 3c. The κ_L constitutes the main factor of κ_{tol} as shown in the inset of Fig. 3c. The electronic contribution is less than 5% because of the low σ. Owing to the ultralow thermal conductivity (0.017 W/mK at 1033 K) of $K_2Ti_6O_{13}$ whiskers, the κ_{tol} of the composites is lower than pure SnSe and a minimum ~0.5 W/mK is obtained with 5 vol% $K_2Ti_6O_{13}$ introduced. The thermoelectric figure of merit ZT ($ZT=S^2\sigma T/\kappa$, T is absolute temperature), for all samples is illustrated in Fig. 3d. Upon

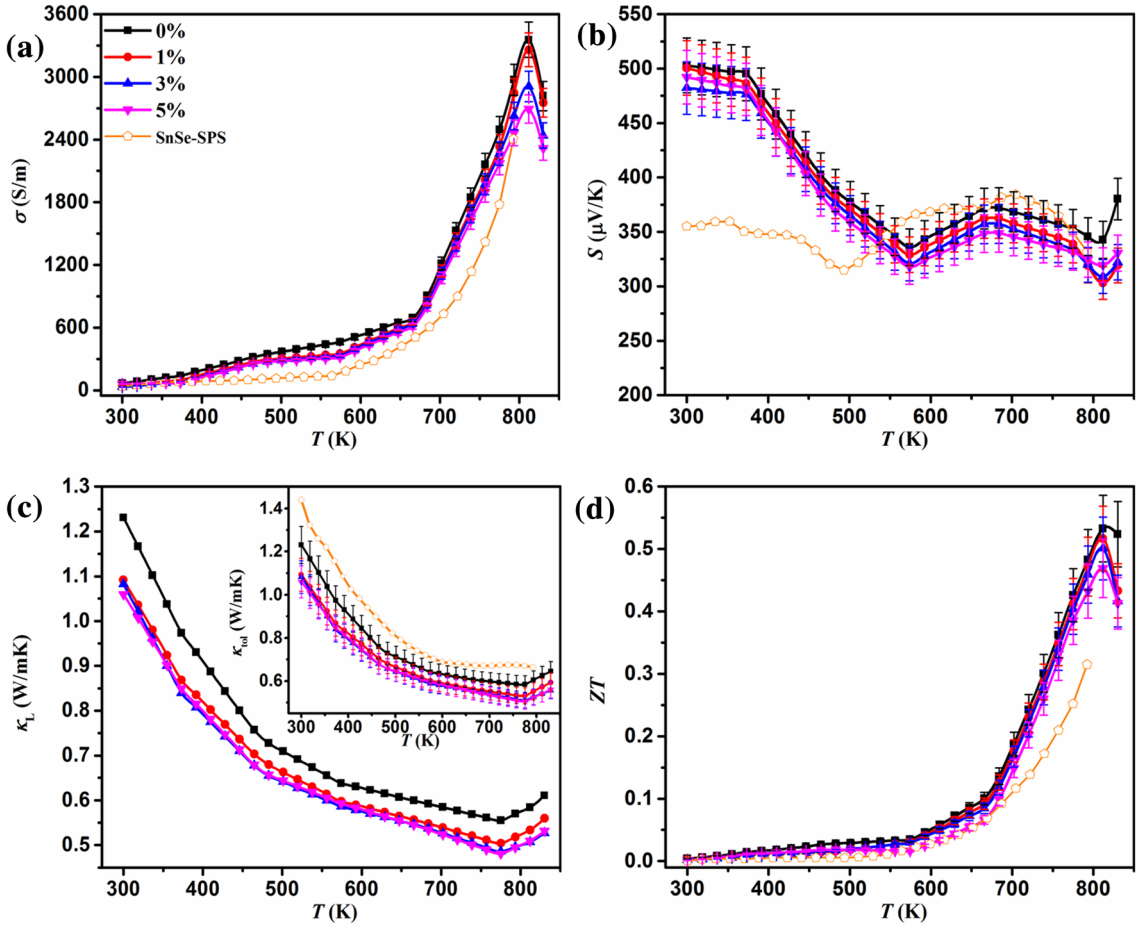

Fig. 3 Temperature dependence of **a** the electrical conductivity σ, **b** the Seebeck coefficient S, **c** lattice thermal conductivity κ_L, and **d** the dimensionless figure of merit ZT. The inset in **c** shows total thermal conductivity κ_{tol}. The data of SnSe-SPS samples are shown for comparison [35]

introducing $K_2Ti_6O_{13}$, the *ZT* values show a slight decrease at elevated temperatures, but still achieves a comparable *ZT* ~ 0.5 at 810 K when 5 vol% $K_2Ti_6O_{13}$ is introduced [13, 37].

3.3 Mechanical properties

Mechanical properties, such as Vickers hardness, flexural strength, compressive strength and fracture toughness of the TE materials must be sufficiently robust to resist the thermal fatigue and stress as well as the potential for fracture, during the TE module in service. All the above mechanical parameters of the composites were improved significantly due to the excellent mechanical properties of $K_2Ti_6O_{13}$, as shown in Fig. 4a–d.

Figure 4a shows that the Vickers hardness increases linearly from 669.3 to 876.6 MPa with $K_2Ti_6O_{13}$ whiskers added, which is much higher than that of SnSe prepared by other methods [12, 13]. A 31% improvement in hardness is obtained by the addition of 5% $K_2Ti_6O_{13}$ whiskers, further evidence that whiskers super strength (Mohs hardness: 4; modulus: 280 GPa) [38] has transferred to the matrix. The tight interface interaction between whiskers and matrix as shown in Fig. 2b–f may be another reason for the enhanced hardness. As shown in Fig. 4b, c, the flexural and compressive strengths of the composites are reached at 41.5 and 78.9 MPa, after introducing 5 vol% $K_2Ti_6O_{13}$ whiskers, representing 98% and 86% improvements, respectively. Figure 4d depicts that the fracture toughness increases from 0.63 to 1.08 MPa $m^{1/2}$ for the samples containing 5 vol% $K_2Ti_6O_{13}$ whiskers, which represents 71% improvement. Compared with other literatures [13], the fracture toughness in this work is much higher. These remarkable enhancements may be owed to the increased plastic deformation of the matrix along the matrix-reinforcement interface, crack branching due to hindrance by reinforcements, and fiber bridging of the crack [39]. This bridging is accompanied by pull-outs of whiskers during fracture of the composites as shown in Fig. 2. The toughening mechanism for the composites containing $K_2Ti_6O_{13}$ whiskers is crack deflection due to the load transfer between

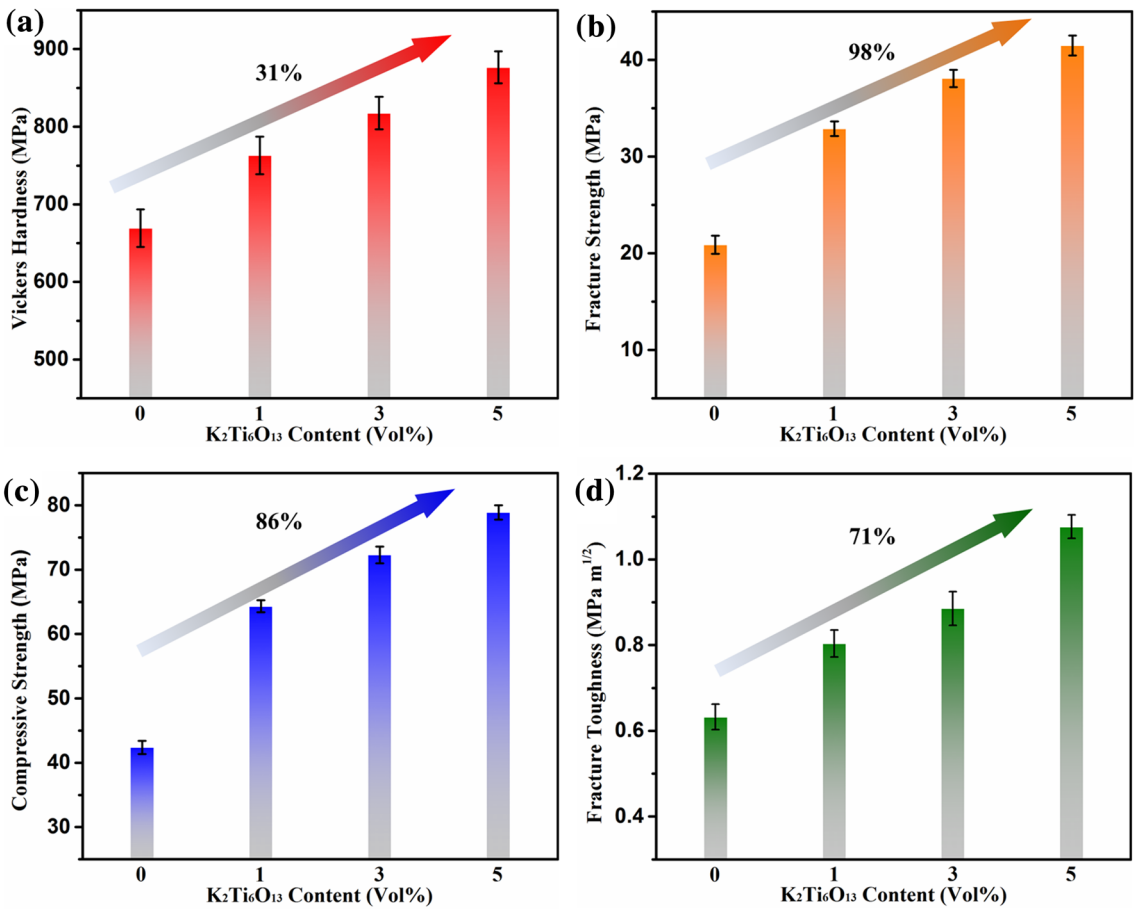

Fig. 4 Room temperature mechanical properties: **a** the Vickers hardness; **b** the flexural strength; **c** the compressive strength; **d** the fracture toughness

$K_2Ti_6O_{13}$ and the matrix while a crack is propagating. All the results indicate that the dispersion of $K_2Ti_6O_{13}$ whiskers is a promising strategy for enhancing the mechanical properties of polycrystalline SnSe and other TE materials.

4 Conclusion

In the present study, a novel reinforcement whisker $K_2Ti_6O_{13}$, with low-cost, high strength, and good dispersibility were firstly introduced to TE materials as the reinforcement phase. These results indicate it is a promising strategy for enhancing the mechanical properties of the SnSe matrix via incorporation of $K_2Ti_6O_{13}$. All the mechanical parameters of the composites have a substantial enhancement. In particular, the flexural strength, compressive strength and fracture toughness were improved by 98%, 86%, and 71% respectively, upon the addition of 5 vol% $K_2Ti_6O_{13}$ whiskers. These whiskers embedded and incorporated with the matrixes which contribute to the significant enhancement of mechanical properties. A further enhancement might be expected if the damage to whiskers is reduced during ball milling and sintering, by using longer whiskers, or by adding whiskers and nanoparticles simultaneously.

Acknowledgements This work was supported by the National Natural Science Foundation of China (Grant No. 51772231), the Fundamental Research Funds for the Central Universities (Grant Nos. WUT: 2018IB002 and 2018IB007) and the Hubei Provincial Natural Science Foundation of China (Grant No. 2018CFB646).

References

1. Y.Z. Pei, A. LaLonde, S. Iwanaga, G.J. Snyder, Energy Environ. Sci. **4**, 2085–2089 (2011)
2. H. Wang, Y. Pei, A.D. Lalonde, G.J. Snyder, Adv. Mater. **23**, 1366–1370 (2011)
3. Q. Zhang, B. Liao, Y. Lan, K. Lukas, W. Liu, K. Esfarjani, C. Opeil, D. Broido, G. Chen, Z. Ren, Proc. Natl. Acad. Sci. **110**, 13261–13266 (2013)
4. L.D. Zhao, S.H. Lo, Y.S. Zhang, H. Sun, G.J. Tan, C. Uher, C. Wolverton, V.P. Dravid, M.G. Kanatzidis, Nature **508**, 373–377 (2014)
5. J.S. Rhyee, K.H. Lee, S.M. Lee, E. Cho, S.I. Kim, E. Lee, Y.S. Kwon, J.H. Shim, G. Kotliar, Nature **459**, 965–968 (2009)
6. K. Ken, Y. Shinsuke, Appl. Phys. Lett. **87**, 804 (2005)
7. G.D. Li, U. Aydemir, M. Wood, W.A.G. III, P.C. Zhai, Q.J. Zhang, G.J. Snyder, Chem. Mater. **29**, 2382–2389 (2017)
8. T.W. Fan, J.L. Ke, L. Fu, B.Y. Tang, L.M. Peng, W.J. Ding, J. Magn. Alloys **1**, 163–168 (2013)
9. G.D. Li, Q. An, U. Aydemir, W.A.G. III, M. Wood, P.C. Zhai, Q.J. Zhang, G.J. Snyder, Chem. Mater. **27**, 6329–6336 (2015)
10. G.D. Li, Q. An, U. Aydemir, W.A.G. III, M. Wood, P.C. Zhai, Q.J. Zhang, G.J. Snyder, J. Mater. Chem. A **4**, 14625–14636 (2016)
11. K. Tyagi, B. Gahtori, S. Bathula, N.K. Singh, S. Bishnoi, S. Auluck, A.K. Srivastava, A. Dhar, RSC Adv. **6**, 11562–11569 (2016)
12. F. Chu, Q.H. Zhang, Z.X. Zhou, D.K. Hou, L.J. Wang, W. Jiang, J. Alloys Compd. **741**, 756–764 (2018)
13. J.F. Fu, X.L. Su, H.Y. Xie, Y.G. Yan, W. Liu, Y.H. You, X. Cheng, C. Uher, X.F. Tang, Nano Energy **44**, 53–62 (2018)
14. B. Duan, P.C. Zhai, P.F. Wen, S. Zhang, L.S. Liu, Q.J. Zhang, Scr. Mater. **67**, 372–375 (2012)
15. T. Akao, Y. Fujiwara, Y. Tarui, T. Onda, Z.C. Chen, J. Electron. Mater. **43**, 2047–2052 (2014)
16. Y. Zheng, W.J. Liu, S.X. Wang, W.H. Xiong, Ceram. Int. **30**, 2111–2115 (2004)
17. P. Wu, Y. Zheng, Y.L. Zhao, H.Z. Yu, Chin. J. Nonferr. Met. **32**, 951–956 (2011)
18. S.Q. Wu, Z.S. Wei, S.C. Tjong, Compos. Sci. Technol. **60**, 2873–2880 (2000)
19. H. Wang, Z.H. Zhang, Z.Y. Hu, F.C. Wang, S.L. Li, E. Korznikov, X.C. Zhao, Y. Liu, Z.F. Liu, Z. Kang, Sci. Rep. **6**, 26258 (2016)
20. X.J. Zhao, D.L. Chen, H.Q. Ru, N. Zhang, J. Eur. Ceram. Soc. **31**, 883–892 (2011)
21. G.S. Zhuang, G.X. Sui, H. Meng, Z.S. Sun, R. Yang, Compos. Sci. Technol. **67**, 1172–1181 (2007)
22. R.Y. Luo, Y.F. Ni, J.S. Li, C.L. Yang, S.B. Wang, Mater. Sci. Eng. **528**, 2023–2027 (2011)
23. M. Sudheer, K. Hemanth, K. Raju, T. Bhat, Proced. Mater. Sci. **6**, 975–987 (2014)
24. L.A. Simpson, Chem. Informationsdienst **57**, 151–154 (1974)
25. Y.J. Fu, J.T. Xu, G.Q. Liu, J. Yang, X.J. Tan, Z. Liu, H.M. Qin, H.Z. Shao, H.C. Jiang, B. Liang, J. Jiang, J. Mater. Chem. C **4**, 1201–1207 (2016)
26. J.C. Li, D. Li, X.Y. Qin, J. Zhang, Scr. Mater. **126**, 6–10 (2017)
27. N.C. Lü, J. Cheng, Y.H. Cheng, Mech. Res. Commun. **32**, 1–14 (2005)
28. I. Levin, W.D. Kaplan, D.G. Brandon, J. Am. Ceram. Soc. **78**, 254–256 (1995)
29. M.D. Thouless, A.G. Evans, Acta Metall. **36**, 517–522 (1988)
30. L.D. Zhao, C. Chang, G.J. Tan, M.G. Kanatzidis, Energy Environ. Sci. **9**, 3044–3060 (2016)
31. T.R. Wei, C.F. Wu, X.Z. Zhang, Q. Tan, L. Sun, Y. Pan, J.F. Li, Phys. Chem. Chem. Phys. **17**, 30102–30109 (2015)
32. B.W. Cai, J.H. Li, H. Sun, P. Zhao, F.R. Yu, L. Zhang, D.L. Yu, Y.J. Tian, B. Xu, J. Alloys Compd. **727**, 1014–1019 (2017)
33. Y.S. Zhang, S.Q. Hao, L.D. Zhao, C. Wolvertonc, Z. Zeng, J. Mater. Chem. A **4**, 12073 (2016)
34. Y.W. Zhang, X.P. Jia, H.R. Sun, B. Sun, B.W. Liu, H.Q. Liu, L.J. Kong, H.A. Ma, J. Alloys Compd. **667**, 123–129 (2016)
35. B.W. Cai, J.H. Li, H. Sun, P. Zhao, F.R. Yu, L. Zhang, D.L. Yu, Y.J. Tian, B. Xu, J. Alloys Compd. **727**, 1014–1019 (2017)
36. J.L. Li, X.L. Zhang, B. Duan, Y.L. Cui, H.J. Yang, H.T. Wang, J.C. Li, X.J. Hu, G. Chen, P.C. Zhai, J. Materiomics (2018). https://doi.org/10.1016/j.jmat.2018.11.002
37. Y.W. Li, F. Li, J.F. Dong, Z.H. Ge, F.Y. Kang, J.Q. He, H.D. Du, B. Li, J.F. Li, J. Mater. Chem. C **4**, 2047–2055 (2016)
38. Y.W. Bao, W. Wang, Y.C. Zhou, Acta Mater. **52**, 5397–5404 (2004)
39. X. Jiang, L.T. Drzal, Polym. Compos. **31**, 1091–1098 (2010)